1
Molecular Catalytic Kinetics Concepts

Rutger A. van Santen

1.1
Key Principles of Heterogeneous Catalysis

We discuss the following topics in the subsequent sections:

- Sabatier principle and volcano curve;
- Brønsted–Evans–Polanyi (BEP) linear activation energy–reaction energy relationships;
- compensation effect in catalytic kinetics;
- micropore size dependence in zeolite catalysis;
- structure sensitivity and insensitivity in transition-metal catalysis;
- transition-state stabilization rules.

The molecular interpretation of major topics in catalytic kinetics will be highlighted based on insights on the properties of transition-state intermediates as deduced from computational chemical density functional theory (DFT) calculations.

1.2
Elementary Rate Constants and Catalytic Cycle

A catalytic reaction is composed of several reaction steps. Molecules have to adsorb to the catalyst and become activated, and product molecules have to desorb. The catalytic reaction is a reaction cycle of elementary reaction steps. The catalytic center is regenerated after reaction. This is the basis of the key molecular principle of catalysis: the Sabatier principle. According to this principle, the rate of a catalytic reaction has a maximum when the rate of activation and the rate of product desorption balance.

The time constant of a heterogeneous catalytic reaction is typically a second. This implies that the catalytic event is much slower than diffusion (10^{-6} s) or

Novel Concepts in Catalysis and Chemical Reactors: Improving the Efficiency for the Future.
Edited by Andrzej Cybulski, Jacob A. Moulijn, and Andrzej Stankiewicz

ISBN: 978-3-527-32469-9

elementary reaction steps ($10^{-4} - 10^{-2}$ s). Activation energies of elementary reaction steps are typically in the order of 100 kJ mol^{-1}. The overall catalytic reaction cycle is slower than elementary reaction steps because usually several reaction steps compete and surfaces tend to be covered with an overlayer of reaction intermediates.

Clearly, catalytic rate constants are much slower than vibrational and rotational processes that take care of energy transfer between the reacting molecules (10^{-12} s). For this reason, transition reaction rate expressions can be used to compute the reaction rate constants of the elementary reaction steps.

Eyring's transition-state reaction rate expression is

$$r_{TST} = \frac{kT}{h}\Gamma\frac{Q^{\#}}{Q_0}e^{-\frac{E_{bar}}{kT}} \tag{1.1a}$$

$$Q = \prod_i \frac{e^{-\frac{1}{2}\frac{h\nu_i}{kT}}}{1 - e^{-\frac{h\nu_i}{kT}}} \tag{1.1b}$$

$Q^{\#}$ is the partition function of transition state and Q_0 is the partition function of ground state, k is Boltzmann's constant, and h is Planck's constant.

The *transition-state energy* is defined as the saddle point of the energy of the system when plotted as a function of the reaction coordinates illustrated in Figure 1.1.

Γ is the probability that reaction coordinate passes the transition-state barrier when the system is in activated state. It is the product of a dynamical correction and the tunneling probability. Whereas statistical mechanics can be used to evaluate the pre-exponent and activation energy, Γ has to be evaluated by molecular dynamics techniques because of the very short timescale of the system in the activated state. For surface reactions not involving hydrogen, Γ is usually close to 1.

Most of the currently used computational chemistry programs provide energies and vibrational frequencies for ground as well as transition states.

A very useful analysis of catalytic reactions is provided for by the construction of so-called *volcano plots* (Figure 1.2). In a volcano plot, the catalytic rate of a reaction normalized per unit reactive surface area is plotted as a function of the adsorption energy of the reactant, product molecule, or reaction intermediates.

A volcano plot correlates a kinetic parameter, such as the activation energy, with a thermodynamic parameter, such as the adsorption energy. The maximum in the volcano plot corresponds to the Sabatier principle maximum, where the rate of activation of reactant molecules and the desorption of product molecules balance.

1.3 Linear Activation Energy–Reaction Energy Relationships

The Sabatier principle deals with the relation between catalytic reaction rate and adsorption energies of surface reaction intermediates. A very useful relation often

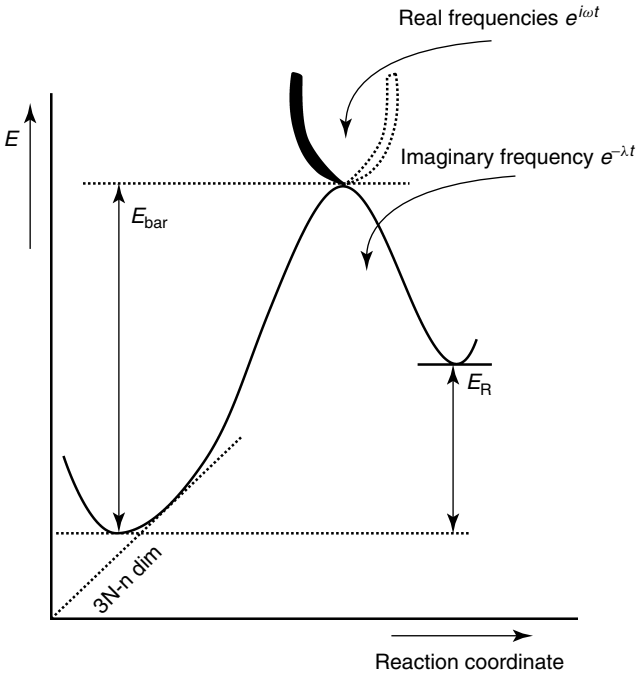

Figure 1.1 Transition-state saddle point diagram. Schematic representation of potential energy as a function of reaction coordinate.

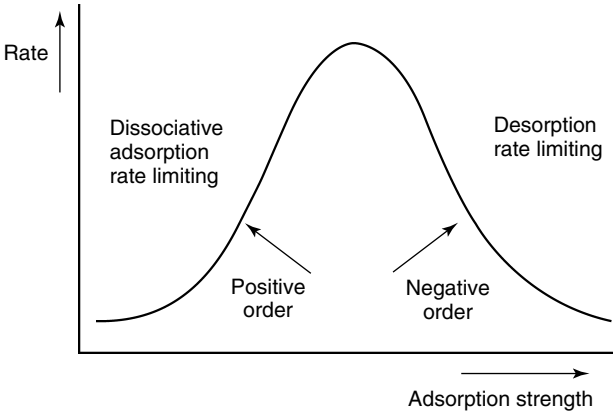

Figure 1.2 Volcano plot illustrating the Sabatier principle. Catalytic rate is maximum at optimum adsorption strength. On the left of the Sabatier maximum, rate has a positive order in reactant concentration, and on the right of Sabatier maximum the rate has a negative order.

exists between the activation energy of elementary surface reaction steps, such as adsorbate bond dissociation or adsorbed fragment recombination and corresponding reaction energies. These give the Brønsted–Evans–Polanyi relations.

For the forward dissociation reaction, the BEP relation is

$$\delta E^{\#}_{\text{diss}} = \alpha \delta E_{\text{react}} \tag{1.2a}$$

Then for the backward recombination reaction Eq. (1.2b) has to hold:

$$\delta E^{\#}_{\text{rec}} = -(1-\alpha)\,\delta E_{\text{react}} \tag{1.2b}$$

Owing to microscopic reversibility, the proportionality constants of the forward and backward reactions are related. These relations are illustrated in Figure 1.3.

The original ideas of Evans and Polanyi [1] to explain such a linear relation between activation energy and reaction energy can be illustrated through a two-dimensional analysis of two crossing potential energy curves.

The two curves in Figure 1.4 represent the energy of a chemical bond that is activated before and after a reaction. The difference between the locations of the potential energy minima is the reaction coordinate x_0.

If one assumes the potential energy curves to have a similar parabolic dependence on the displacement of the atoms, a simple relation can be deduced between activation energy, the crossing point energy of the two curves, and the reaction energy. One then finds for α:

$$E_{\text{act}} = E^{\circ}_{\text{act}} \left(\frac{\Delta E_r}{4E^{\circ}_{\text{act}}} + 1 \right)^2 \tag{1.3a}$$

$$\alpha = \frac{\delta E_{\text{act}}}{\delta E_r} = \frac{1}{2}\left(1 + \frac{\Delta E_r}{4E^{\circ}_{\text{act}}}\right) \tag{1.3b}$$

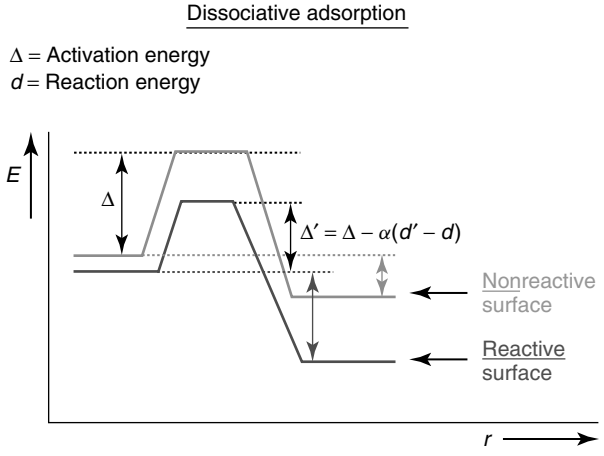

Figure 1.3 Illustration of the BEP relation $\Delta' = \Delta - \alpha\,(d' - d)$.

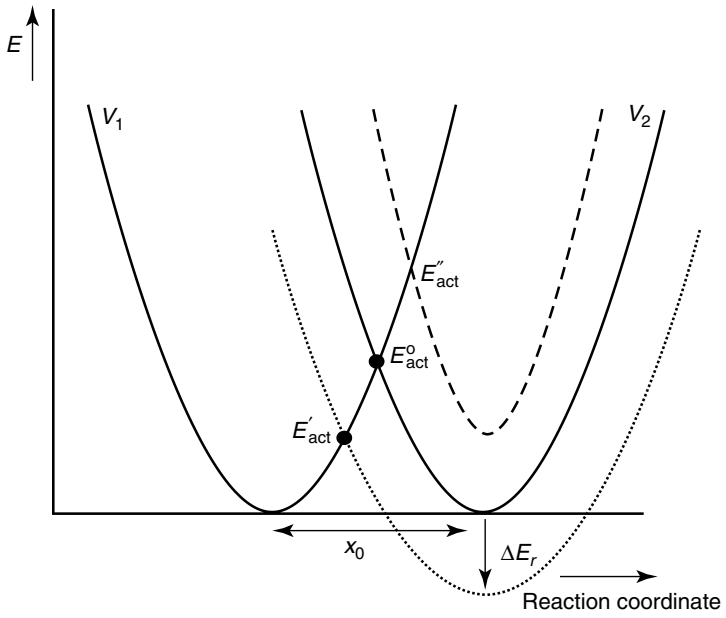

Figure 1.4 Two-dimensional curve-crossing potential energy diagram of reacting system with similar potential energies before and after reaction (schematic).

One notes that the proportionality constant, α, depends on the reaction energy, ΔE_r. Therefore, Eq. (1.3) is not strictly a linear relation between activation energy change and reaction energy. In the extreme limit of high exothermicity of the reaction energy $\alpha = 0$, and the crossing point of the two curves is at the minimum of curve V_1. In this case the transition state is called *early*. Its structure is close to that of the reactant state.

In the limit of high endothermicity $\alpha = 1$ and now the crossing point is close to the minimum of curve V_2. The transition-state structure is now close to that of the final state. The transition state can now be considered to be late. This analysis is important, since it illustrates why α varies between 0 and 1. Often α is simply assumed to be equal to 0.5.

The BEP relation is only expected to hold as long as one compares systems in which the reaction path of the reacting molecules is similar. An illustration is provided in Figure 1.5 [2].

In this figure, the activation energies of N_2 dissociation are compared for the different reaction centers: the (111) surface structure of an fcc crystal and a stepped surface. Activation energies with respect to the energy of the gas-phase molecule are related to the adsorption energies of the N atoms. As often found for bond activating surface reactions, a value of α close to 1 is obtained. It implies that the electronic interactions between the surface and the reactant in the transition state and product state are similar. The bond strength of the chemical bond

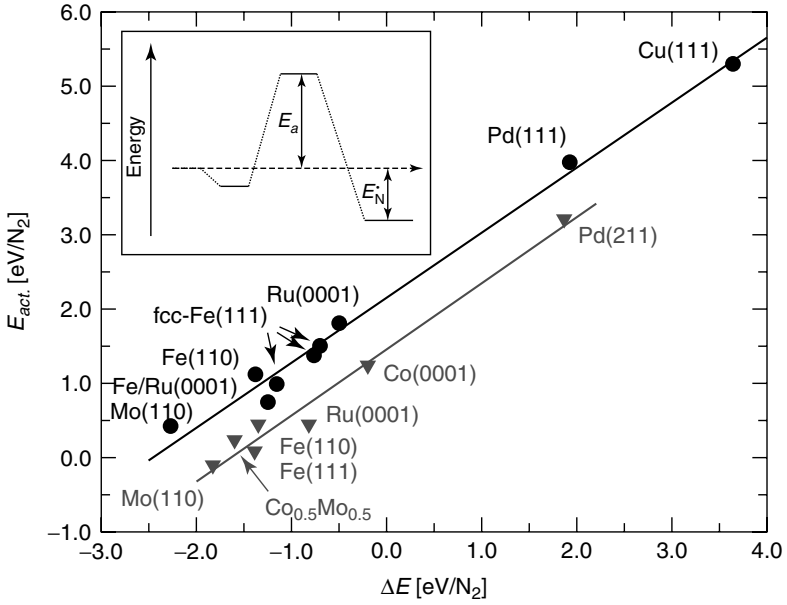

Figure 1.5 Plot of computed reaction barriers for dissociation at $E_{act.}$ for N_2 dissociation as a function of nitrogen atom adsorption energy on surface terrace and stepped surface [2]. The upper curve is for surface terrace of (111) type of fcc crystals, and the lower curve presents data on the stepped surfaces.

that is activated is substantially weakened due to the strong interaction with the metal surface. The structure of the transition state is close to that of the product state.

This is illustrated in Figure 1.6 for the dissociation of CO [3]. As a consequence of the high value of α, the proportionality constant of recombination is usually approximately 0.2, reflecting a weakening of the adatom surface bonds in transition state by this small amount. It implies that typically one of the six surface bonds is broken in the transition state compared to the adsorption state of the two atoms before recombination.

1.4 Microkinetic Expressions; Derivation of Volcano Curve

In microkinetics, overall rate expressions are deduced from the rates of elementary rate constants within a molecular mechanistic scheme of the reaction. We will use the methanation reaction as an example to illustrate the

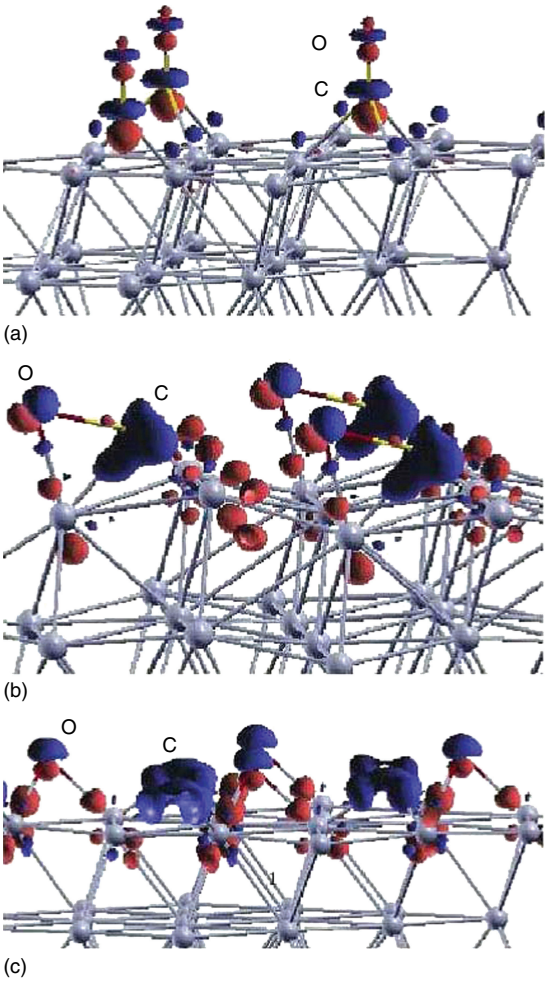

Figure 1.6 Structures and electron density changes of dissociating CO on Ru(0001) surface: (a) adsorbed CO, (b) transition state for dissociation, and (c) dissociated state.

physicochemical basis of the Sabatier volcano curve. The corresponding elementary reactions are

$$CO_g \underset{k_{diss}}{\overset{k_{ads}}{\rightleftharpoons}} CO_{ads} \tag{1.4a}$$

$$CO_{ads} \xrightarrow{k_{diss}} C_{ads} + O_{ads} \tag{1.4b}$$

$$C_{ads} + 2H_2 \xrightarrow[r_H]{} CH_4 \nearrow \tag{1.4c}$$

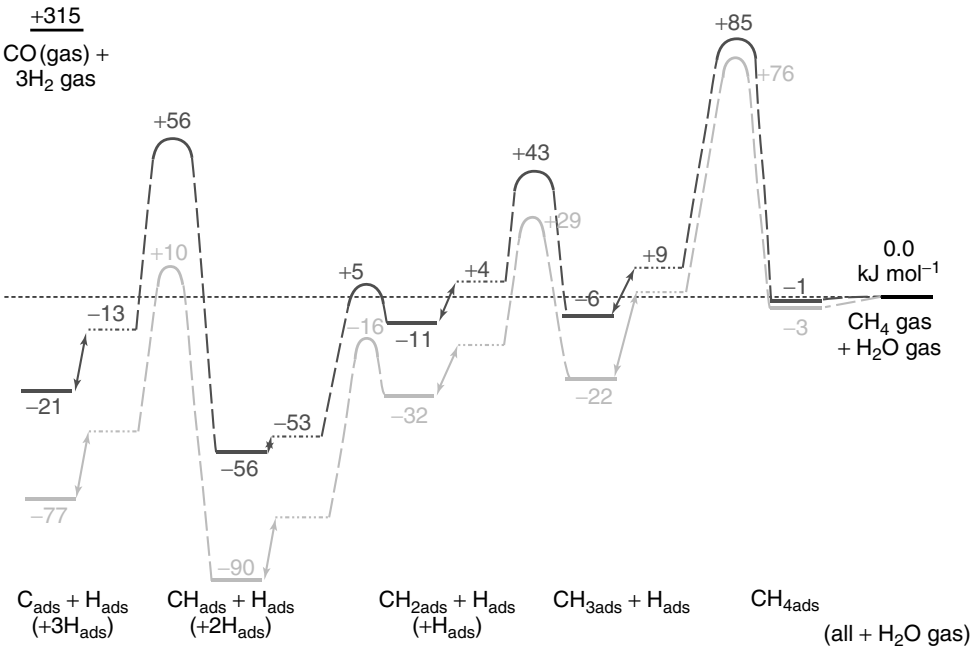

Figure 1.7 Reaction scheme of reaction of C_{ads} with H_{ads} to produce CH_4 on Ru(0001) surface. Coverages of 25% and 11% are compared. Energies with respect to gas phase [4].

Surface carbon hydrogenation occurs through a sequence of hydrogenation steps in which $CH_{x,ads}$ species are formed with increasing hydrogenation. r_H, the rate of C_{ads} hydrogenation, depends implicitly on hydrogen pressure.

For Ru(0001) the corresponding reaction energy scheme is shown in Figure 1.7 [4]. The relative energies of the different reaction intermediates, C_{ads} or CH_{ads}, may strongly depend on the type of surface and metal. When for different surfaces or metals the relative interaction with H_{ads} increases C_{ads} may for instance become more stable than CH. This is found for more coordinative unsaturated surfaces or more reactive metals.

We present expressions for reaction rates and steady-state concentrations using the simplified assumption that C_{ads} hydrogenation to CH_4 occurs in one reaction step. We also assume that O_{ads} removal is fast and that hydrogen adsorption is not influenced by the other adsorbates.

Then the activation energy for methane production from C_{ads} is the overall activation energy for the hydrogenation of C_{ads} to CH_4, and Eq. (1.5) gives the rate of methane production:

$$R_{CH_4} = r_H \cdot \theta_c \tag{1.5}$$

A closed expression for θ_C can be deduced:

$$\theta_C = 1 + \frac{1}{2}\lambda - \frac{1}{2}\sqrt{\lambda^2 + 4\lambda} \tag{1.6a}$$

$$\approx \frac{1}{1+\lambda} \tag{1.6b}$$

with

$$\lambda = \frac{r_H}{k_{diss}} \frac{\left(K_{ads}^{CO} \cdot [CO] + 1\right)^2}{\left(K_{ads}^{CO}[CO]\right)} \tag{1.7a}$$

$$= A\frac{r_H}{k_{diss}} \tag{1.7b}$$

One notes that the coverage of C_{ads} depends on two important parameters: the ratio ρ of the rate of hydrogenation of C_{ads} to give methane and the rate constant of CO dissociation:

$$\rho = \frac{r_H}{k_{diss}} \tag{1.8}$$

and the equilibrium constant of CO adsorption, K_{eq}^{CO}. The coverage with C_{ads} increases with decreasing value of ρ. This implies a high rate of k_{diss} and slow rate of C_{ads} hydrogenation. The strong pressure dependence of CO relates to the need of neighboring vacant sites for CO dissociation.

Beyond a particular value of K_{eq}^{CO} the surface coverage with C_{ads} decreases because CO dissociation becomes inhibited.

In order to proceed, one needs to know the relation between the rate constants and reaction energies. This determines the functional behavior of ρ.

We use the linear activation energy–reaction energy relationships as deduced from the BEP relation and write expressions for k_{diss}, r_H, and λ:

$$k_{diss} = \nu_0 e^{-\frac{E_{diss}^0}{kT}} \cdot e^{-\alpha\frac{E'_{ads}}{kT}} \tag{1.9a}$$

$$= \nu_0' e^{-\alpha'\frac{E_{ads}}{kT}} \tag{1.9b}$$

$$r_H = r_H' e^{x\frac{E_{ads}}{kT}} \tag{1.9c}$$

$$\lambda = A\frac{r_H'}{\nu_0'} e^{(x+\alpha')\frac{E_{ads}}{kT}} \tag{1.10}$$

The dissociation rate of CO_{ads} will increase with increasing exothermicity of the reaction energy. One can use the adsorption energy of the carbon atom as the standard measure.

From chemisorption theory we know that adatom adsorption energies will decrease in a row of the periodic system of the group VIII metals when the position of the element moves to the right. The rate of hydrogenation of C_{ads} will decrease with increasing adsorption energy of C_{ads} and hence will decrease in the same order with element position in the periodic system.

We now study the consequences of these BEP choices to the dependence of predicted rate of methane production on E_{ads}. Making the additional simplifying assumption that the adsorption energy parameters in Eqs. (1.9b) and (1.9c) are the same, one finds for the rate of methane production an expression

$$R_{CH_4} = C\frac{\lambda^{\frac{x}{x+\alpha'}}}{1+\lambda} \tag{1.11a}$$

with

$$C = r'_H\left(\frac{r'_H}{r'_0}A\right)^{-\frac{x}{x+\alpha'}} \tag{1.11b}$$

In Eq. (1.11b) the constant A depends on the equilibrium constant K_{eq}^{CO}. This will vary also with the adsorption energy of C or O, but will be much less sensitive to these variations than the activation energies of CO dissociation and hydrogenation [5].

The dependence of R_{CH_4} on λ is sketched in Figure 1.8.

Equation (1.11a) will have only a maximum as long as

$$\frac{x}{x+\alpha'} < 1 \tag{1.12}$$

Within our model this condition is always satisfied. We find an interesting result that the Sabatier volcano maximum is found when

$$\lambda_{max} = \frac{x}{\alpha'} \tag{1.13}$$

The controlling parameters that determine the volcano curve are the BEP constants: k_{diss} and r_H. It is exclusively determined by the value of ρ. It expresses the compromise of the opposing elementary rate events: dissociation versus product

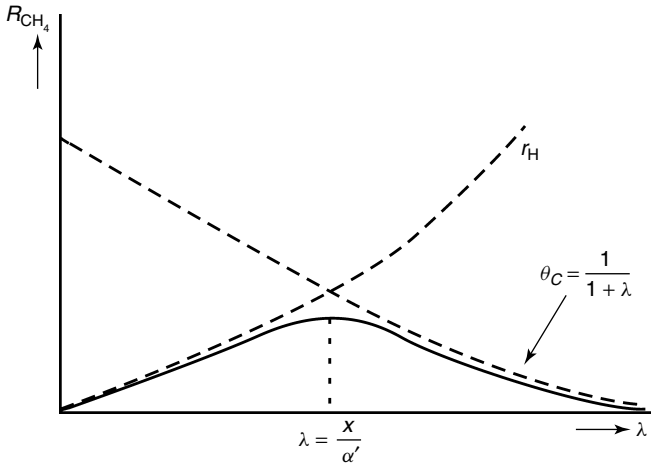

Figure 1.8 Dependence of R_{CH_4} on λ (schematic).

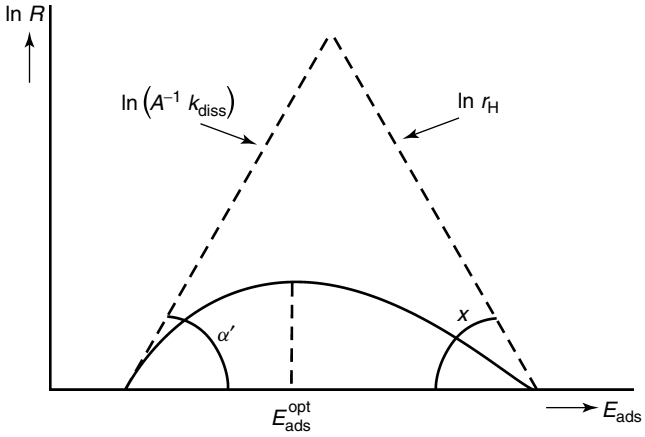

Figure 1.9 Volcano curve dependence of rate of methanation, R, on E_{ads} (schematic).

formation. The CO partial pressure determines the dependence of the rate on gas-phase pressure. It controls λ through changes of parameter A. Note that variation of A would also give volcano-type behavior. This is obviously found when the rate is plotted as a function of gas-phase pressure A. It relates to the blocking of surface sites by increasing adsorption of CO molecules. Volcano-type behavior is illustrated in Figure 1.9 for constant CO pressure.

Equation (1.5) then allows us to deduce the optimum value of E_{ads} of the Sabatier maximum rate. It can be deduced from Eq. (1.12a). The latter depends on the CO pressure through A.

The volcano curve is bounded by the rate of dissociative adsorption of CO and hydrogenation of adsorbed carbon. This is illustrated in Figure 1.9.

For relevant related treatments see [6]. Whereas the above discussion limits itself to the conversion of CO to a single product, the treatment can be easily extended to a selectivity problem.

Interestingly, one can easily deduce an expression for the relative rate of coke formation as compared to that of methanation. The rate of initial coke formation depends on the combination probability of carbon atoms and hence is given by

$$R_{C-C} = r_{CC} \cdot \theta_C^2 \tag{1.14}$$

The relative rate of coke versus methane formation then follows from

$$\frac{R_{CC}}{R_{CH_4}} = \frac{r_{CC} \cdot \theta_C^2}{r_H \cdot \theta_C} \tag{1.15a}$$

$$= \frac{r_{CC}}{r_H} \cdot \theta_C \tag{1.15b}$$

Interestingly as we have seen this may have a maximum as a function of the metal–carbon bond energy.

The occurrence of a maximum depends on the BEP parameter α'' of the C–C bond formation rate. Volcano-type behavior for the selectivity is found as long as

Eq. (1.16a) is satisfied.

$$2x + \alpha > \alpha'' > x \tag{1.16a}$$

Then,

$$\lambda_{\max}^{\text{sel}} = \frac{\alpha'' - x}{2x + \alpha - \alpha''} \tag{1.16b}$$

r_{CC} and r_H decrease when the carbon adsorption energy increases. Volcano-type behavior of the selectivity to coke formation is found when the activation energy of C–C bond formation decreases faster with increasing metal–carbon bond energy than with the rate of methane formation. Equation (1.16b) indicates that the rate of the nonselective C–C bond forming reaction is slow when θ_C is high and when the metal–carbon bond is so strong that methane formation exceeds the carbon–carbon bond formation. The other extreme is the case of very slow CO dissociation, where θ_C is so small that the rate of C–C bond formation is minimized.

This analysis indicates the importance of a proper understanding of BEP relations for surface reactions. It enables a prediction not only of conversion rates but also of selectivity trends.

1.5 Compensation Effect

For catalytic reactions and systems that are related through Sabatier-type relations based on kinetic relationships as expressed by Eqs. (1.5) and (1.6), one can also deduce that a so-called *compensation effect* exists. According to the compensation effect there is a linear relation between the change in the apparent activation energy of a reaction and the logarithm of its corresponding pre-exponent in the Arrhenius reaction rate expression.

The occurrence of a compensation effect can be readily deduced from Eqs. (1.6) and (1.7). The physical basis of the compensation effect is similar to that of the Sabatier volcano curve. When reaction conditions or catalytic reactivity of a surface changes, the surface coverage of the catalyst is modified. This change in surface coverage changes the rate through change in the reaction order of a reaction.

In Eq. (1.5) the surface coverage is given by θ_C, and θ_C is related to parameter λ of Eq. (1.7). Equation (1.5) can be rewritten to show explicitly its dependence on gas-phase concentration. Equation (1.17a) gives the result. This expression can be related to practical kinetic expressions by writing it as a power law as is done in Eq. (1.18b). Power-law-type rate expressions present the rate of a reaction as a function of the reaction order. In Eq. (1.17b) the reaction order is m in H_2 and $-n$ in CO.

$$R_H = \frac{r_H k_{diss} K_{ads}^{CO} [CO]}{k_{diss} K_{ads}^{CO} [CO] + r_H \left(K_{ads}^{CO} [CO] + 1\right)^2} \tag{1.17a}$$

$$\approx k_H^l k_{diss}^{-n} \left(K_{ads}^{CO}\right)^{-n} [CO]^{-n} [H_2]^m$$

$$l \leq 1 \tag{1.17b}$$

Power law expressions are useful as long as the approximate orders of reactant concentration are constant over a particular concentration course. A change in the order of the reaction corresponds to a change in the surface concentration of a particular reactant. A low reaction order usually implies a high surface concentration, a low reaction order, and a low surface reaction of the corresponding adsorbed intermediates. In order to deduce (Eq. (1.17b)) the rate of surface carbon hydrogenation, the power law of Eq. (1.18) has been used.

$$r_{\mathrm{H}} = k_{\mathrm{H}} \cdot [\mathrm{H}_2]^t \,;\, m = t \cdot l \tag{1.18}$$

From Eq. (1.17b) the apparent activation energy as well as the pre-exponent can be readily deduced. They are given in Eq. (1.19).

$$\begin{aligned} E_{\mathrm{app}} &= lE_{\mathrm{act}}^{\mathrm{H}} - n\left\{E_{\mathrm{act}}(\mathrm{diss}) + E_{\mathrm{ads}}\,(\mathrm{CO})\right\} && (1.19a)\\ &= lE_{\mathrm{act}}^{\mathrm{H}} - n\Delta E_{\mathrm{app}} \\ \ln A_{\mathrm{app}} &= \ln \Gamma \cdot \frac{ekT}{h} + \frac{l}{k}\Delta S_{\mathrm{act}}^{\mathrm{H}} - \frac{n}{k}\Delta S_{\mathrm{app}} && (1.19b)\\ \Delta S_{\mathrm{app}} &= \Delta S_{\mathrm{act}}\left(\mathrm{diss}\right) + \Delta S_{\mathrm{ads}}(\mathrm{CO}) && (1.19c) \end{aligned}$$

The orders of the reaction appear as coefficients of activation energies and adsorption energies and their corresponding entropies. For more detailed discussions see [7].

A consequence of the compensation effect is the presence of an isokinetic temperature. For a particular reaction, the logarithm of the rate of a reaction measured at different conditions versus $1/T$ should cross at the same (isokinetic) temperature. For conditions with varying n, this isokinetic temperature easily follows from Eq. (1.19) and is given by

$$T_{\mathrm{iso}} = \frac{\Delta E_{\mathrm{app}}}{k\Delta S_{\mathrm{app}}} \tag{1.20}$$

It is important to realize that the compensation effect in catalysis refers to the overall catalytic reactions.

The activation energies of elementary reaction steps may sometimes show a relationship between activation energy changes and activation entropies.

A reaction with a high activation energy tends to have a weaker interaction with the surface and hence will have enhanced mobility that is reflected in a larger activation entropy. For this reason, the pre-exponents of surface desorption rate constants are 10^4-10^6 larger than the pre-exponents of surface reaction rates.

In classical reaction rate theory expressions, this directly follows from the frequency–pre-exponent relationship:

$$k_{\mathrm{class}} = \nu \frac{r_t^2}{r_i^2} e^{-\frac{E_{\mathrm{act}}}{kT}} \tag{1.21}$$

A high frequency of vibration between surface and reactant implies a strong bond, which will give a high activation energy. Hence, increase in pre-exponent and corresponding activation energies counteract. Equation (1.21) is the rate expression

for a weakly bonded complex. The bond frequency is ν, and r_i and r_t are the initial and transition-state radii. Equation (1.21) is valid for a freely rotating diatomic complex.

Compensation-type behavior is quite general and has been extensively studied, especially in transition-metal catalysis [8a], sulfide catalysis [8b], and zeolite catalysis [7].

In the next section, we present a short discussion of compensation-type behavior in zeolite catalysis.

1.6 Hydrocarbon Conversion Catalyzed by Zeolites

As a further illustration of the compensation effect, we use solid-acid-catalyzed hydrocarbon activation by microporous zeolites. A classical issue in zeolite catalysis is the relationship between overall rate of a catalytic reaction and the match of shape and size between adsorbate and zeolite micropore.

For a monomolecular reaction, such as the cracking of hydrocarbons by protonic zeolites, the rate expression is very similar to the one in Eq. (1.5). The rate of the reaction is now proportional to the concentration of molecules at the reaction center, the proton of the zeolite, Eq. (1.22a).

$$r = k_{act} \cdot \theta \tag{1.22a}$$

$$= k_{act} \cdot \frac{K_{eq}[C_H]}{1 + K_{eq}[C_H]} \tag{1.22b}$$

Assuming adsorption to behave according to the Langmuir adsorption isotherm, we get Eq. (1.22b). Both the rate constant of proton activation k_{act} and the equilibrium constant of adsorption K_{eq} depend on cavity details.

Quantum-chemical studies have indeed shown that the presence of a surrounding cavity lowers the barriers of charge separation that occur when a molecule is activated by zeolitic protons [9] as shown in Figure 1.10.

The presence of the zeolite cavity dramatically lowers the activation energy for the protonation of toluene. It is mainly due to screening of the charges in the transition state due to the polarizable lattice oxygen atoms. In the transition state, a positive charge develops on protonated toluene.

This reduction in activation energy will occur only when the structure of the transition state complex fits well in the zeolite cavity. This is the case for the protonated toluene example in the zeolite mordenite channel. The structure of the transition state complex in the cluster simulation and zeolite can be observed to be very similar to the one in Figure 1.10.

The activation energy will be strongly increased when there is a mismatch between transition-state-complex shape and cavity. The rate constant then typically behaves as indicated in the following equation:

$$k_{act} = k_{act}^{n,st} e^{\frac{\Delta G_{st}}{kT}} \tag{1.23}$$

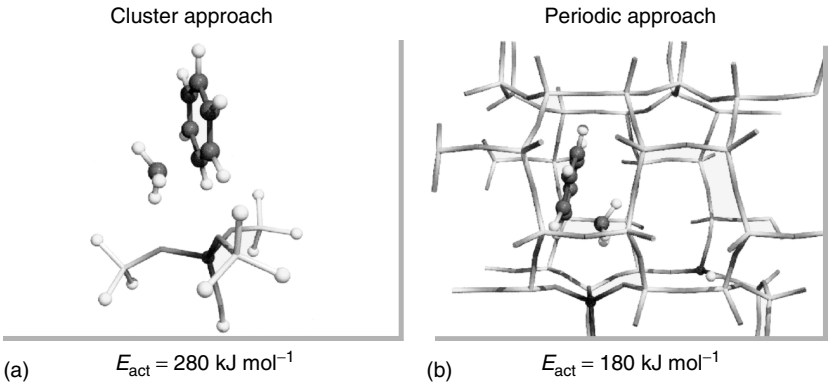

Figure 1.10 Comparison of the activation energy of protonation of toluene by (a) an acidic cluster versus that of activation of the same molecule by (b) Mordenite (MOR) [9a].

ΔG_{st} is the difference in free energy due to steric constants in reactant and transition state. $k^{n,st}$ is the rate constant of the nonsterically constrained reaction. The contribution of the steric component to the transition-state energy cannot be deduced accurately from DFT calculations because van der Waals energies are poorly computed. Force field methods have to be used to properly account for such interactions.

For adsorption in zeolites, the biased Monte Carlo method as developed by Smit is an excellent method to determine the free energies of molecules adsorbed on zeolites [9b]. This method can be used to compute the concentration of molecules adsorbed on zeolites, as we discuss below.

We will use this method to deduce ΔG_{st} for hydrogen transfer reaction. The free energies of adsorption of reacting molecules such as propylene and butane are compared with the free energies of reaction intermediate molecules that are analogous to the intermediates formed in the transition state. A C–C bond replaces the C–H–C bond. An example of such a transition state and analog intermediate is given in Figure 1.11.

In Table 1.1 a comparison is made of the differences in free energies for two different zeolites. Note the large repulsive energies computed for the intermediates and their sensitivity to zeolite structure.

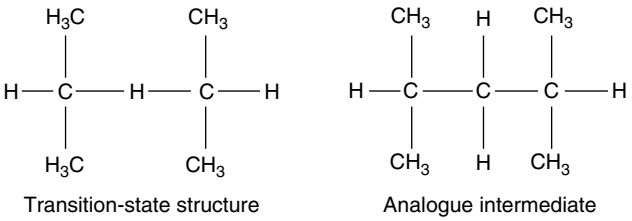

Figure 1.11 Transition state for hydrogen transfer and its analog intermediate (schematic).

Table 1.1 Configurationally biased Monte Carlo simulations of the adsorption enthalpies of hydrocarbons for two zeolites.

	ΔH_{ads} (kJmol^{-1})	
	MFI	**Chabasite**
Propane	−41.0	−34.6
n-Butane	−44.1	−47.0
C_6	−50.7	−65.1
C_8	−49.9	−43.1
$\Delta E(C_6 - 2C_3)$	+31.3	+4.1
$\Delta E(C_8 - 2C_4)$	+38.3	+50.9

An alternative view to interpreting ΔG_{st} is the realization that reactants before getting activated to a particular reaction have to be present in a conformation such that a particular reaction can occur. The actual activation of reacting molecule or molecules is not strongly affected by this state. Calculations on the activation of the different isomers of xylene have indeed demonstrated that differences in the energies of the pretransition-state configurations dominate the activation energy differences [10], and hence the Maxwell–Boltzmann term, Eq. (1.23), has to be interpreted as the relative probability that a particular intermediate pretransition-state structure is realized in zeolite [11].

This is the reason that for complex cracking reactions in zeolites the product pattern can be predicted from a simulation of the free energies of the corresponding intermediate molecules in the zeolite [11].

As long as there are no important steric contributions to the transition-state energies, the elementary rate constant of Eq. (1.22) does not sensitively depend on the detailed shape of the zeolite cavity. Then the dominant contribution is due to the coverage dependent term θ.

This has been demonstrated by a comparison of the cracking rates of small linear hydrocarbons in ZSM-5 [12] and also for reactions in different zeolites for the hydroisomerization of hexane [13]. Differences in catalytic conversion appear to be mainly due to differences in θ.

The apparent activation energies can be deduced from Eq. (1.22b). The corresponding expression is given by Eq. (1.24a):

$$E_{app} = E_{act} + E_{ads}(1 - \theta) \tag{1.24a}$$

$$r \approx k_{act} K_{eq}^{(1-\theta)} [C_H]^{1-\theta} \qquad 0 < \theta < 1 \tag{1.24b}$$

In the absence of steric constraints in Eq. (1.24a) E_{act} will not vary. E_{ads} and θ are the parameters that significantly change with hydrocarbon chain length or zeolite.

Table 1.2 Calculated heats of adsorption and adsorption constants for various hydrocarbons in zeolites with different channel dimensions.

	ΔH_{ads}(kJ mol^{-1})	K_{ads}(T = 513K) (mmol (g Pa)$^{-1}$)
	Simulation	**Simulation**
n-Pentane/TON	−63.6	4.8×10^{-6}
n-Pentane/MOR	−61.5	4.8×10^{-5}
n-Hexane/TON	−76.3	1.25×10^{-5}
n-Hexane/MOR	−69.5	1.25×10^{-4}

Since the interaction of linear hydrocarbons is dominated by the van der Waals interaction with the zeolite, the apparent activation energies for cracking decrease linearly with chain length. In some cases, differences in the overall rate are not dominated by differences in the heat of adsorption but instead are dominated by differences in the enthrones of adsorbed molecules.

One notes in Table 1.2 a uniform increase in the adsorption energies of the alkanes when the microspore size decreases (compare 12-ring-channel zeolite MOR with 10-ring-channel TON). However, at the temperature of hydroisomerization the equilibrium constant for adsorption is less in the narrow-pore zeolite than in the wide-pore system. This difference is due to the more limited mobility of the hydrocarbon in the narrow-pore material. This can be used to compute Eq. (1.22b) with the result that the overall hydroisomerization rate in the narrow-pore material is lower than that in the wide-pore material. This entropy-difference-dominated effect is reflected in a substantially decreased hydrocarbon concentration in the narrow-pore material.

1.7
Structure Sensitive and Insensitive Reactions

A classical issue in transition-metal catalysis is the dependence of catalytic activity on changes in the particle size of the metal clusters in the nanosize region [14].

As illustrated in Figure 1.12, three types of behavior can be observed. The most significant surface feature that changes with metal particle size is the ratio of corner, edge, and terrace surface atoms.

The increase in the rate of case II is related with an increase in the relative ratio of the edge and corner atoms over the decreasing number of terrace atoms. This increase in reactivity relates to the increased degree of coordinative unsaturation of the edge and corner atoms.

Important changes in the electronic structure occur. Electron delocalization decreases, which is reflected in a narrowing, especially, of the d-valence electron

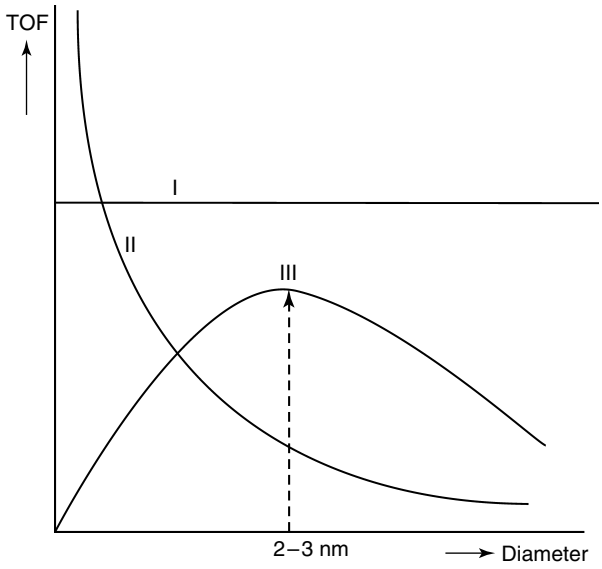

Figure 1.12 The three different types of cluster size dependence of catalytic conversion. Rates are considered normalized per exposed surface atom (schematic).

bands and a corresponding upward shift of the d-valence electron band center due to increased electron–electron interactions [5].

The decrease in bandwidth is proportional to

$$\sqrt{N_s} \tag{1.25}$$

Within the tight binding approximation, it implies a decrease in electron localization energy:

$$\Delta E_{\text{loc}} \approx \left(\sqrt{N'_S} - \sqrt{N_S}\right)\beta \tag{1.26}$$

for the surface atom with the lowest number of nearest neighbor surface atoms N'_S compared to that of a surface atom with N_s neighbors. β is a measure of the interatomic overlap energy.

The dependence on electron localization energy can also be illustrated by the use of the bond order conservation principle. This principle gives an approximate recipe to estimate changes in bond strength when coordination of a surface atom or adsorbate attachment changes [5, 15].

According to this principle, the valence of an atom is considered a constant. When more atoms coordinate to the same atom, the valence has to be distributed over more bonds, and hence the strength per bond decreases. When the chemical bonds are equivalent, the bond strength of an individual bond $\varepsilon(n)$ depends in the following way on the corresponding bond strength of a complex with a single

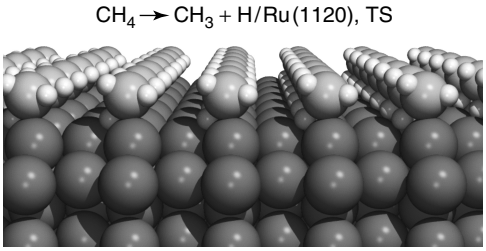

Figure 1.13 Transition-state configuration of methane activation on Ru(1120) surface.

bond (ε_0):

$$\varepsilon\,(n) = \varepsilon_0 \left(\frac{2n-1}{n^2}\right) \tag{1.27}$$

n is the total number of bonds with the metal atom. The surface atom metal coordination number is given by

$$N = n - 1 \tag{1.28}$$

Class II dependence for the activation of a chemical bond as a function of surface metal atom coordinative unsaturation is typically found for chemical bonds of σ character, such as the CH or C–C bond in an alkane. Activation of such bonds usually occurs atop of a metal atom. The transition-state configuration for methane on a Ru surface illustrates this (Figure 1.13).

The data presented in Table 1.3 illustrate the dependence of the activation energy of methane on the edge or corner (kink) atom position of some transition-metal surfaces.

The BEP α value for methane activation is close to 1. As a consequence of the BEP value for hydrogenation of adsorbed methyl, the reverse reaction should be nearly zero.

The dependence on decreasing particle size that results for this recombination reaction is the same as Class I in Figure 1.12. The differences between the activation

Table 1.3 Methane activation on edge and corner atoms (kilojoules per mol).

Ru(0001)[a]	76
Ru(1120)[b]	56
Rh(111)[c]	67
Rh step[c]	32
Rh kink[c]	20
Pd(111)[c]	66
Pd step[c]	38
Pd kink[c]	41

[a] (0001) Ciobica *et al.* [4].
[b] (1120) Ciobica and van Santen [16].
[c] Liu and Hu [17].

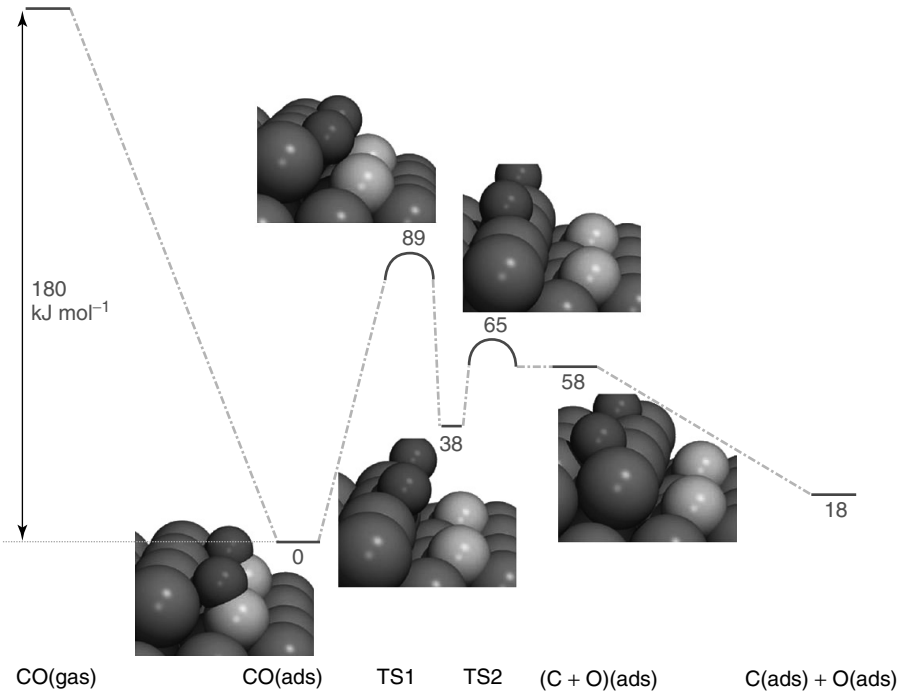

Figure 1.14 Energetics (kilojoules per mole) and structure of CO dissociating from Ru step-edge site [16].

energies for dissociation hence closely relate to the differences in energy of the adsorbed product fragments $methyl_{ads}$ and H_{ads}. The rate of this recombination reaction has become independent of surface atom coordination number.

Class II and Class I behavior are found to be closely related and are each other's complement. In practical catalysis, Class I behavior is typically found for hydrogenation reactions.

Class III-type behavior is representative of reactions in which π bonds have to be broken. It is the typical behavior of reactions in which CO or N_2 bond activation is rate limiting.

The activation energy of such molecules depends strongly on the structure of the catalytically active center. The structures of reactant, transition state as well as product state at a step-edge site are shown for CO dissociation in Figure 1.14.

Surface step-edge sites have substantially lowered activation energies compared to the activation energies of the same dissociation reactions on surface terraces (compare 91 kJ mol^{-1} in Figure 1.14 with 215 kJ mol^{-1} on Ru(0001) surface). This lowered barrier is due to several factors that affect chemical bonding. Because of multiple contacts of the CO molecule at the step-edge site, there is substantially more back donation into the CO bond weakening $2\pi^*$ orbitals. As a consequence of stretching the CO bond to its transition-state distance, only a small extension is

required. Thirdly, in the transition state the oxygen and carbon atoms do not share bonding with the same surface metal atom. Such sharing is an important reason for enhanced barrier energies at terraces (due to the bond order conservation principle).

This is discussed more extensively in the next section.

Whereas the adsorption energies of the adsorbed molecules and fragment atoms only slightly change, the activation barriers at step sites are substantially reduced compared to those at the terrace. Different from activation of σ-type bonds, activation of π bonds at different sites proceeds through elementary reaction steps for which there is no relation between reaction energy and activation barrier. The activation barrier for the forward dissociation barrier as well as for the reverse recombination barrier is reduced for step-edge sites.

Interestingly, when the particle size of metal nanoparticles becomes less than 2 nm, terraces become so small that they cannot anymore support the presence of step-edge site metal atom configurations. This can be observed from Figure 1.15, which shows a cubo-octahedron just large enough to support a step-edge site.

Class III-type behavior is the consequence of this impossibility to create step-edge-type sites on smaller particles. Larger particles will also support the step-edge sites. Details may vary. Surface step directions can have a different orientation and so does the coordinative unsaturation of the atoms that participate in the ensemble of atoms that form the reactive center. This will enhance the activation barrier compared to that on the smaller clusters. Recombination as well as dissociation reactions of π molecular bonds will show Class III-type behavior.

The different BEP behavior for the activation of σ versus π bonds, basic to the very different Class I and Class II particle size dependence compared to Class III particle size dependence, is summarized in Figure 1.16 [14].

Whereas Class I and Class II behavior are intrinsically related through microscopic reversibility, Class III-type behavior implies that there is no BEP relation between the changes in activation energy and structure.

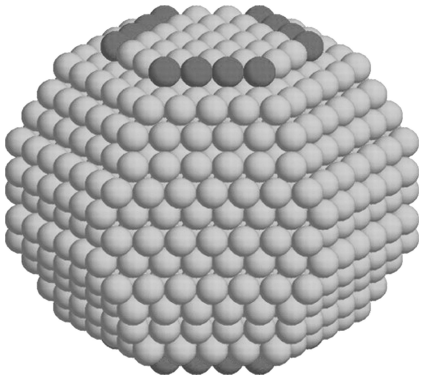

Figure 1.15 Cubo-octahedron with step-edge sites [18].

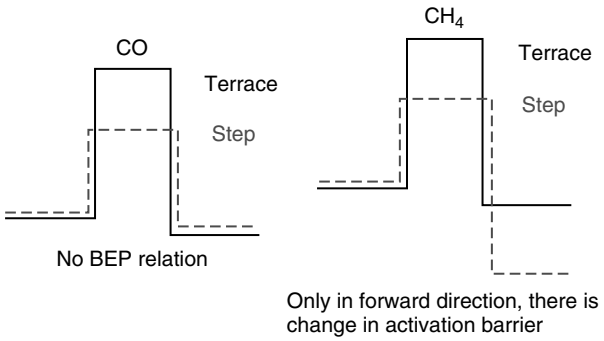

Figure 1.16 Changes in methane versus CO activation barriers as a function of surface structure (schematic).

When the selectivity of a reaction is controlled by differences in the way molecules are activated on different sites, the probability of the presence of different sites becomes important. An example again can be taken from the activation of CO. For methanation, activation of the CO bond is essential. This will proceed with low barriers at step-edge-type sites. If one is interested in the production of methanol, catalytic surfaces are preferred, which do not allow for easy CO dissociation. This will typically be the case for terrace sites. The selectivity of the reaction to produce methanol will then be given by an expression as in Eq. (1.29a):

$$S = \frac{x_1 r_1}{x_1 r_1 + x_2 r_2} \tag{1.29a}$$

$$\frac{r_1}{r_2} = \frac{r_{CH_3OH} \cdot \theta_{CO}}{k_{diss} \theta_{CO} (1 - \theta)} \approx \frac{r_{CH_3OH}}{k_{diss}} \left(1 + K_{ads}^{CO} [CO]\right) \tag{1.29b}$$

In this expression, x_1 and x_2 are the fractions of terrace versus step-edge sites, r_1 is net rate of conversion of adsorbed CO to methanol on a terrace site, and r_2 is the rate of CO dissociation at a step-edge-type site. Increased CO pressure will also enhance the selectivity, because it will block dissociation of CO.

1.8
The Nonmetal Atom Sharing Rule of Low-Barrier Transition States

1.8.1
Introduction

As we discussed in the previous section, the primary parameter that determines the interaction strength between an adsorbate and a (transition) metal surface is the coordinative unsaturation of the surface metal atoms. The lower the coordination number of a surface atom, the larger the interaction with interacting adsorbates.

We discussed that for methane activation this leads to lowering of the activation energy compared to the reactivity of terrace, edge, or corner atoms successively.

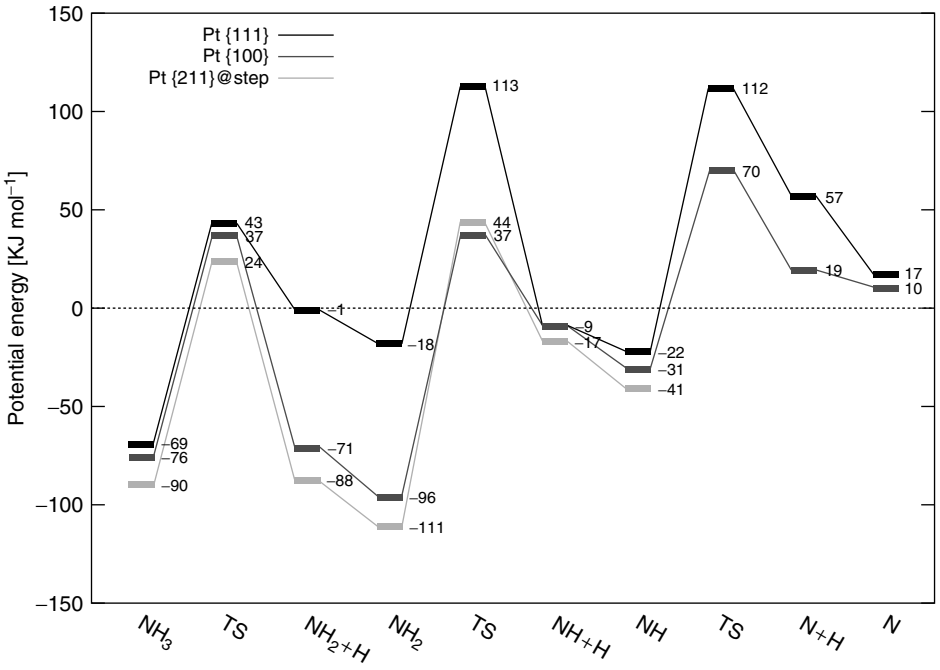

Figure 1.17 Reaction energy diagram of NH_3 activation compared on different surfaces (energies in kilojoules per mole).

Very important to this behavior is the cleavage of the CH bond over a single metal atom.

This trend in activation energy decrease with increasing degree of surface atom unsaturation is not general. It does not apply to the activation energies of NH_3 or H_2O activation, notwithstanding that again essentially only the interaction with a single surface metal atom is relevant and the bonds to be activated are also σ-type bonds.

The trend is illustrated for ammonia activation in Figure 1.17 [19]. In this figure, the activation energies of ammonia activation are compared for stepped and nonstepped surfaces of Pt. Similarly as also found for H_2O activation [20], the dissociation barrier is found to be invariant to surface structural changes. This is very different compared to the earlier discussed activation of methane that shows a very strong structural dependence.

It is due to the already significant surface atom–molecule interaction present in the case of ammonia and water before reaction, when the molecules adsorb strongly through their respective molecular lone-pair orbitals.

During the stretching of the XH bond, the molecule maintains its original coordination. Only when the XH bond is broken, the surface NH_2 or OH fragment may move to a higher coordination site.

Whereas now the bond cleavage reaction is nonsurface dependent, the reverse reaction clearly is. The stronger the NH_2 and NH fragments bind, the higher the barrier for the recombination reaction. In the case of methane activation we found the reverse situation. Both situations are consistent with microscopic reversibility.

Interestingly, this situation is very different when we consider activation of NH_3 or H_2O by coadsorbed O. This would typically occur in the Ostwald reaction that oxidizes ammonia to NO or the methane reforming reaction in which CH_4 reacts with O_2 or H_2O to give CO, CO_2, and H_2.

Ammonia activation by Pt, to be discussed in the next section, is an interesting example, because it illustrates the basic principle that provides chemical direction to the identification of surface topologies that give low reaction barriers in surface reactions. This holds specifically for elementary reactions that require a surface ensemble of atoms.

The next section introduces the topological concept of low-barrier transition states through the prevention of formation of shared bonds between reacting surface adsorbates and surface metal atoms.

1.8.2 Ammonia Oxidation

Figure 1.18 compares the activation energies of direct activation of NH_3 and its activation by coadsorbed O on Pt(111) [21]. As can be observed in this figure, reaction with coadsorbed O only lowers the barrier for NH_3 activation by coadsorbed O. The other NH_x intermediates have similar activation energies in the absence of coadsorbed oxygen.

The key difference between the activation energies of the NH_3–O interaction on the (111) surface and the interaction with the other NH_2 fragments is the different topology of the corresponding transition states. Since only NH_3 adsorbs atop, but oxygen requires higher coordination, only the transition state of NH_3–O is realized without binding to the same metal atom of the surface fragment nitrogen atom and coadsorbed O. Competitive adsorption to the same metal atom weakens the adsorbate bonds, and hence a repulsive interaction between reacting fragments arises. The essential chemical bonding feature on which this effect is based is bond order conservation, as discussed before in the context of the explanation of the increase in chemical reactivity with decreased surface atom coordination.

The difference in reactivity of adsorbed NH_x fragments with O as observed by a comparison of Figures 1.18 and 1.19 is striking. On the (100) surface, the activation of the NH_x fragments with x equal to 2 or 1 is also decreased when reacting with coadsorbed O.

As can be seen from Figure 1.20 [22], those transition states that do not share binding to the same surface metal atom have low barriers. The fcc(100) surface has the unique property that the reaction can occur through motion over the square hollow with bonds that remain directed toward the corner atoms of the square atom arrangement on the surface. This is a unique and important feature of reactions that require in their transition states interactions with several surface atoms.

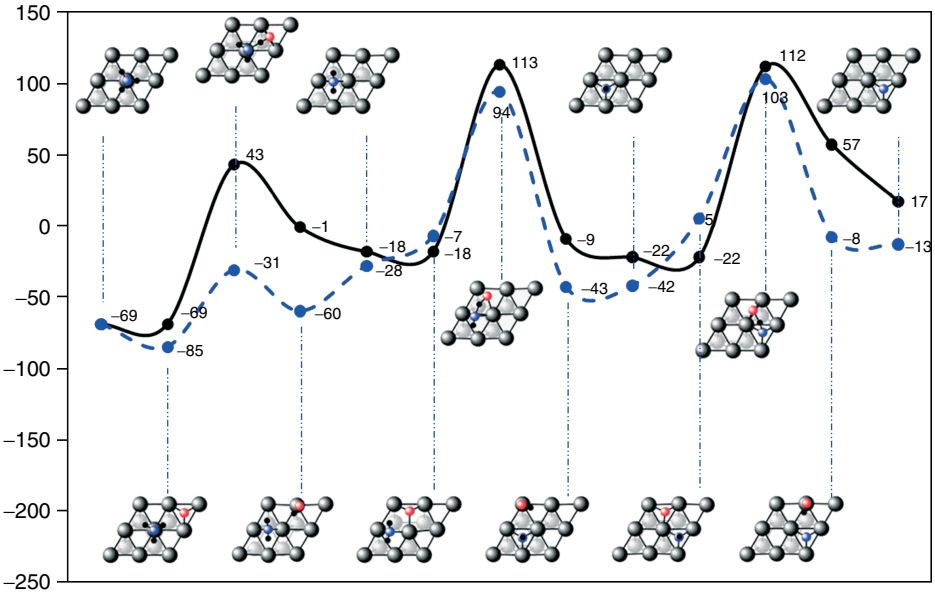

Figure 1.18 Reaction energy diagram that compares direct NH_3 activation and NH_3 (–) activation through reaction with adsorbed O (– – –) on Pt(111) and the corresponding structures for direct NH_3 activation (energies in kilojoules per mole).

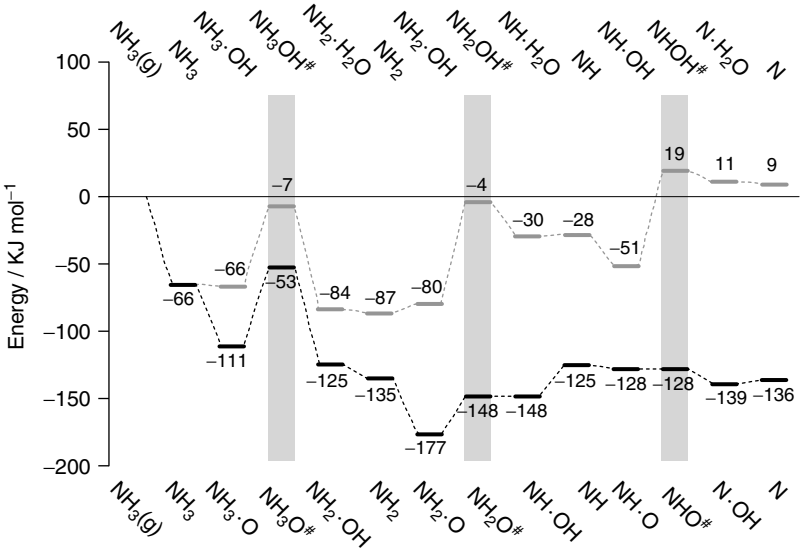

Figure 1.19 Reaction energy diagram of NH_3–O and NH_3–OH activation on Pt(100) [22].

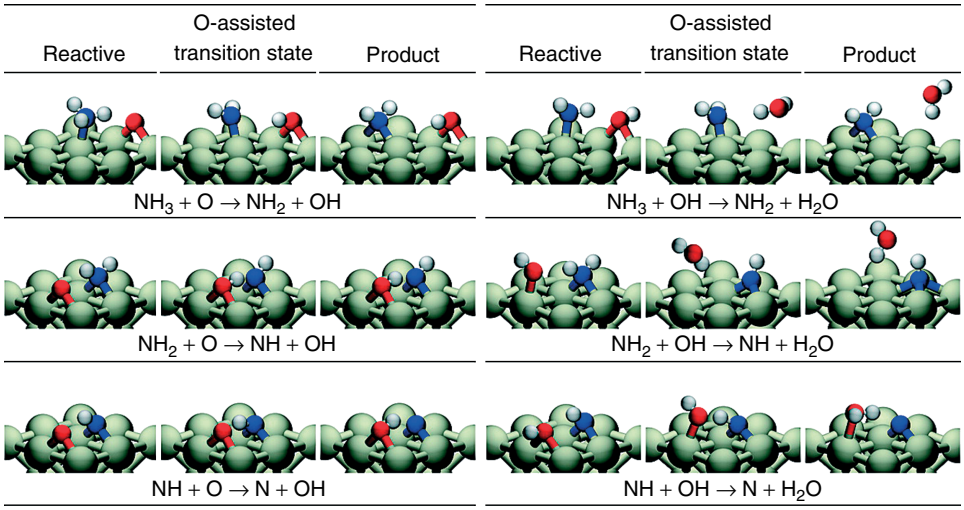

Figure 1.20 The structures of reaction intermediates that correspond to Figure 1.19 [22].

This is characteristic for the activation of molecular π bonds. The same principle was found to apply for stepped surfaces. It is also characteristic of other reactions with surface fragments that have strong repulsive interactions when they share binding with the same surface atom, for example, NH and O, which typically prefer bonding in high-coordination sites.

The relevance of the same nonsurface metal atom sharing principle in transition states is nicely illustrated by the similar lowering of the transition state for NH activation by O in a step site as for the (100) surface, as illustrated in Figure 1.21 [19]. Similarly, OH formation by recombination of oxygen and hydrogen is substantially lower at a step edge than on the (111) terrace.

The kinetics of H–O recombination is very important in the reforming reaction of methane to produce CO and H_2. When more weakly bonded O_{ads} recombines with H_{ads} (preferred on Pt), the main product next to CO will be H_2. On planar Rh with a stronger M–O bond interaction, this reaction is suppressed and therefore H_2 is the main product [23]. Clearly this selectivity will be dramatically affected by the presence of surface steps.

Figure 1.22 schematically summarizes the principle of the preferred transition states without sharing of a common metal atom. Whereas we have earlier discussed surface sensitivity as a function of the relative ratio of particle surface edge sites and surface terrace atoms, the discussion given above provides a principle for particle size shape differences.

Particles of face centered cubic (FCC) crystal would be exclusively terminated by (100) surfaces, whereas cubo-octahedron-type particles may have a dominance of the more stable (111) surfaces.

As first noted by Neurock *et al.* [24], the Pt(100) surface provides sites for extremely low barriers of NO and N_2 recombination. For NO, the energetics on

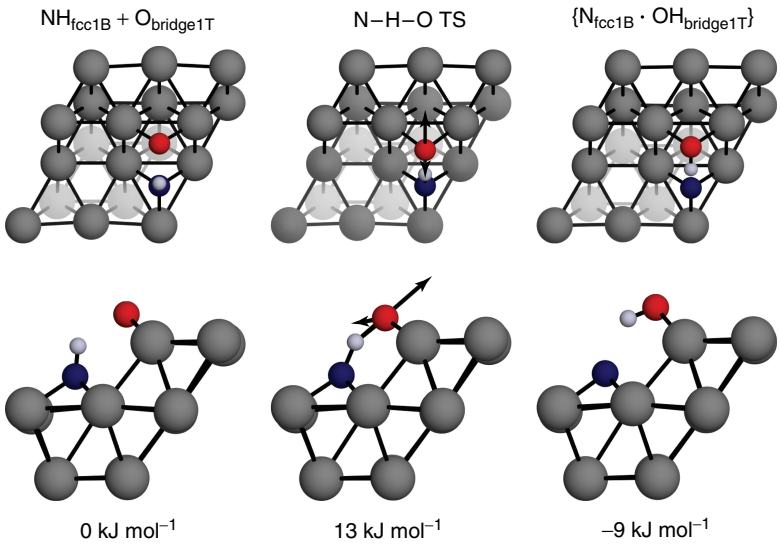

Figure 1.21 Structures and relative energies of NH_{ads} and O_{ads} reaction intermediates along {211}Pt step.

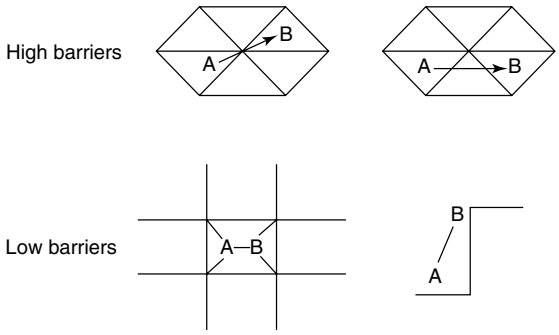

Figure 1.22 Structures of high-barrier and low-barrier transition states of surface bond cleavage reactions.

different surfaces is compared in Figure 1.23. The barriers for recombination to give NO are low on (100) surfaces but higher on the stepped as well as nonstepped (111) surfaces. The lower barrier on the (100) surface compared to the stepped (111) surface is due to destabilization of N_{ads} on the (111) compared to the (100) surface. N_{ads} prefers triangular coordination.

The adsorption energy of N_2 is also low, but that of NO on the (100) surface is substantial. Notwithstanding the very similar activation energies for N_2 and NO formation (see Tables 1.4 and 1.5), the strong interaction of NO with both surfaces implies that the selectivity of the reaction toward N_2 will be high at low temperatures. The NO once formed will not desorb and can only be removed as N_2O.

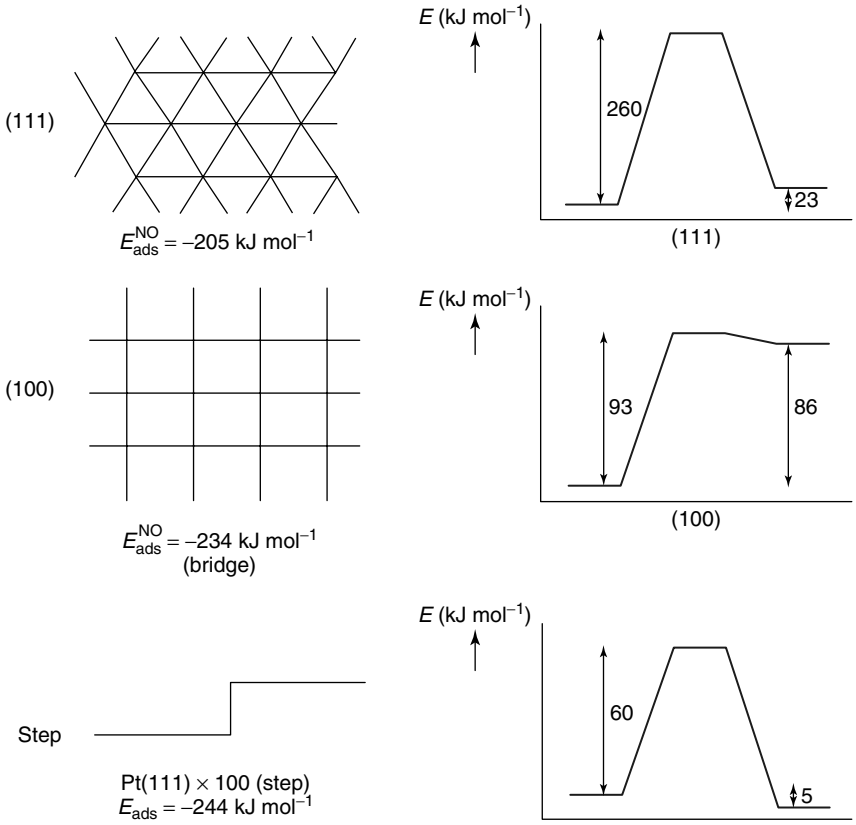

Figure 1.23 A comparison of NO activation on the (111), (100), and stepped (111) surface.

Table 1.4 The activation energies on the Pt(100) surface.

	E_{act} (kJ mol^{-1})
$N + N \rightarrow N_{2gas}$	36
$N + O \rightarrow NO_{ads}$	20
$NO_{ads} \rightarrow NO_{gas}$	204
$N_a + NO_a \rightarrow N_2O_{gas}$	67

At low temperatures, reaction towards N_2 and N_2O product formation preferentially occurs at the (100) surface, and hence a significant particle shape sensitivity is predicted. At higher temperatures when NO readily desorbs, overall activation barriers on the different surfaces tend to become similar and hence surface sensitivity becomes less. The high selectivity toward NO at higher temperatures relates

Table 1.5 The activation energies on the Pt (111) surface.

	E_{act} (kJ mol^{-1})
$N + N \rightarrow N_{2gas}$: Pt(111)	148
$N + O \rightarrow NO_{ads}$: Pt(111)	189
$NO_{ads} \rightarrow NO_{gas}$	187

to the rapid reaction of N_{ads} with coadsorbed O, whose coverage dominates and hence competitive N_2 formation has a slow rate.

1.9 Summary

Using microkinetic expressions, we have discussed the most important catalytic concepts that describe heterogeneous catalytic reactions. We have related these concepts with the energies, entropies, and transition-state features that are accessible through current state-of-the-art DFT techniques.

Whereas it is very useful to relate reaction mechanistic proposals with catalytic kinetics, one has to be aware that DFT-predicted energies typically have an error of at least 10 kJ mol^{-1}.

Predictive kinetics requires accuracies that are an order of magnitude more precise. There are many examples that predict overall kinetics quite accurately. This is then due to a fortuitous cancellation of errors that needs to be understood well for each case.

We did not extensively discuss the consequences of lateral interactions of surface species adsorbed in adsorption overlayers. They lead to changes in the effective activation energies mainly because of consequences to the interaction energies in coadsorbed pretransition states. At lower temperatures, it can also lead to surface overlayer pattern formation due to phase separation. Such effects cannot be captured by mean-field statistical methods such as the microkinetics approaches but require treatment by dynamic Monte Carlo techniques as discussed in [25].

References

1. Evans, M.G. and Polanyi, M. (1938) *Trans. Faraday Soc.*, **34**, 11.
2. Dahl, S., Logadottir, A., Jacobsen, C.J.H., and Nørskov, J.K. (2001) *Appl. Catal. A Gen.*, **222**, 19.
3. Shetty, S.G., Jansen, A.P.J., and van Santen, R.A. (2008) *J. Phys. Chem. C*, **112**, 14027.
4. Ciobica, I.M., Fréchard, F., van Santen, R.A., Kleijn, A.W., and Hafner, J. (2000) *J. Phys. Chem. B*, **104**, 3364.
5. van Santen, R.A. and Neurock, M. (2006) *Molecular Heterogeneous Catalysis*, Wiley-VCH Verlag GmbH, Weinheim.
6. (a) Bligaard, T., Nørskov, J.K., Dahl, S., Matthiesen, J., Christensen, C.M., and

Sehested, J. (2004) *J. Catal.*, **222**, 206; (b) Kaszetelan, S. (1992) *Appl. Catal. A Gen.*, **83**, L1.
7. Bond, G.C., Keane, M.A., Kral, H., and Lercher, J.A. (2000) *Catal. Rev.-Sci. Eng.*, **42** (3), 323.
8. (a) Bligaard, T., Honkala, K., Logadottir, A., Nørskov, J.R., Dahl, S., and Jacobson, C.J.H. (2007) *J. Phys. Chem. B*, **107**, 9325; (b) Toulhoat, H. and Raybaud, P. (2003) *J. Catal.*, **216**, 63.
9. (a) Rozanka, X. and van Santen, R.A. (2004) in *Computer Modelling of Microporous Materials*, Chapter 9 (eds C.R.A. Catlow, R.A. van Santen, and B. Smit), Elsevier; (b) Smit, B. (2004) in *Computer Modelling of Microporous Materials*, Chapter 2 (eds C.R.A.Catlow, R.A. van Santen, and B. Smit), Elsevier.
10. Vos, A.M., Rozanska, X., Schoonheydt, R.A., van Santen, R.A., Hutschka, F., and Hafner, J. (2001) *J. Am. Chem. Soc.*, **123**, 2799.
11. Smit, B. and Maesen, T.L.M. (2008) *Nature*, **451**, 671.
12. (a) Haag, W.O. (1994), in *Zeolites and Related Microporous Materials: State of the Art 1994 Chapter V* (eds J. Weitkamp, H.G. Karge, H. Pfeifer, and W. Hölderick), Elsevier, p. 1375; (b) Narbeshuber, Th.F., Vinety, H., and Lercher, J. (1995) *J. Catal.*, **157**, 338.
13. de Gauw, F.J.J.M.M., van Grondelle, J., and van Santen, R.A. (2002) *J. Catal.*, **206**, 295.
14. van Santen, R.A. (2008) *Acc. Chem. Res.*, **42**, 57.
15. Shustorovich, E. (1990) *Adv. Catal.*, **37**, 101.
16. Ciobica, I.M. and van Santen, R.A. (2002) *J. Phys. Chem. B*, **106**, 6200.
17. Liu, Z.-P. and Hu, P. (2003) *J. Am. Chem. Soc.*, **125**, 1958.
18. Honkala, K., Hellman, A., Remediakis, I.N., Logadottir, A., Carlsson, A., Dahl, S., Christensen, C.H., and Nørskov, J.K. (2005) *Science*, **307**, 555.
19. Offermans, W.K., Jansen, A.P.J., van Santen, R.A., Novell-Leruth, G., Ricart, J., and Pérez-Ramirez, J. (2007) *J. Phys. Chem. B*, **111**, 17551.
20. van Grootel, P.W., Hensen, E.J.M., and van Santen, R.A., submitted.
21. (a) Offermans, W.K., Jansen, A.P.J., and van Santen, R.A. (2006) *Surf. Sci.*, **600**, 1714; (b) Baerns, M., Imbihl, R., Kondratenko, V.A., Kraehert, R., Offermans, W.K., van Santen, R.A., and Scheibe, A. (2005) *J. Catal.*, **232**, 226; (c) van Santen, R.A., Offermans, W.K., Ricart, J.M., Novell-Leruth, G., and Pérez-Ramirez, J. (2008) *J. Phys.: Conf. Ser.*, **117**, 012028.
22. Novell-Leruth, G., Ricart, J.M., and Pérez-Ramírez, J. (2008) *J. Phys. Chem. C*, **112**, 13554.
23. Hickman, D.A. and Schmidt, L. (1993) *Science*, **249**, 343.
24. Ge, Q. and Neurock, M. (2004) *J. Am. Chem. Soc.*, **126**, 1551.
25. Gelten, R.J., van Santen, R.A., and Jansen, A.P.J. (1999) in *Molecular Dynamics, from Classical to Quantum Methods*, Chapter 18 (eds P.B. Balbuena and J.M. Seminario), Elsevier Science B.V.